

# Measuring stellar oscillations using equivalent widths of absorption lines

T. R. Bedding,<sup>1</sup> H. Kjeldsen,<sup>2,3</sup> J. Reetz<sup>4</sup> and B. Barbuy<sup>5</sup>

<sup>1</sup>*Chatterton Astronomy Department, School of Physics, University of Sydney 2006, Australia (bedding@physics.usyd.edu.au)*

<sup>2</sup>*Teoretisk Astrofysik Center, Danmarks Grundforskningsfond*

<sup>3</sup>*Institute of Physics and Astronomy, Aarhus University, DK-8000 Aarhus C, Denmark*

<sup>4</sup>*Institut für Astronomie und Astrophysik der Universität München, Scheinerstr. 1, D-81679 München, Germany*

<sup>5</sup>*Universidade de São Paulo, IAG, Depto. de Astronomia, CP 9638, São Paulo, 01065-970, Brazil*

29 July 2018

## ABSTRACT

Kjeldsen et al. (1995) have developed a new technique for measuring stellar oscillations and claimed a detection in the G subgiant  $\eta$  Boo. The technique involves monitoring temperature fluctuations in a star via their effect on the equivalent width of Balmer lines. In this paper we use synthetic stellar spectra to investigate the temperature dependence of the Balmer lines, Ca II, Fe I, the Mg b feature and the G band. We present a list of target stars likely to show solar-like oscillations and estimate their expected amplitudes. We also show that centre-to-limb variations in Balmer-line profiles allow one to detect oscillation modes with  $\ell \leq 4$ , which accounts for the detection by Kjeldsen et al. of modes with degree  $\ell = 3$  in integrated sunlight.

**Key words:** stars: oscillations – Sun: oscillations – Sun: atmosphere – stars: individual:  $\eta$  Boo (HR 5235) – stars: individual:  $\alpha$  Cen A (HR 5459) –  $\delta$  Scuti.

## 1 INTRODUCTION

Measuring stellar oscillations is extremely difficult. The five-minute oscillations in the Sun, while rich in their information content, have tiny amplitudes. Observing similar oscillations in other stars therefore poses a great challenge (see Brown & Gilliland 1994 for a recent review). Most attempts have sought to detect periodic Doppler shifts of spectral lines. A second method involves measuring the total stellar luminosity, which varies due to changes in temperature induced by acoustic waves in the stellar atmosphere. Kjeldsen et al. (1995; hereafter referred to as KBVF) have proposed a new method in which they measure temperature changes via their effect on the equivalent widths of the Balmer hydrogen lines. They presented strong evidence for oscillations in the G subgiant  $\eta$  Boo (see also Bedding & Kjeldsen 1995), with frequency splittings that were later found to agree with theoretical models (Christensen-Dalsgaard et al. 1995a; Christensen-Dalsgaard, Bedding & Kjeldsen 1995b).

Here we examine the equivalent-width method in more detail. In Section 2 we use synthetic spectra to calculate the temperature sensitivity of the Balmer lines and other strong absorption features. In Section 3 we use these results to estimate oscillation amplitudes for a list of target stars. In Section 4 we discuss the centre-to-limb behaviour of absorption lines and show that observing Balmer-line equivalent widths allows one to detect non-radial oscillation modes with  $\ell \leq 4$ .

## 2 TEMPERATURE DEPENDENCE OF EQUIVALENT WIDTHS

The amplitude of an oscillation when measured in equivalent width ( $W$ ) is related to the temperature fluctuations via

$$\frac{\delta W}{W} = \frac{\partial \ln W}{\partial \ln T} \frac{\delta T}{T}. \quad (1)$$

Lines that are highly sensitive to temperature can be used to measure oscillations, while temperature-insensitive lines are useful as references. Also, detection sensitivity can be improved by combining observations of different lines, but only if the temperature dependence is known for each one.

To determine the function  $W(T)$ , we shall assume that an oscillating star can be represented at all times by a model atmosphere in radiative equilibrium. A more sophisticated approach would require that the acoustic waves be treated explicitly (see Breger 1975 and Frandsen 1984). With this assumption, we may calculate  $W(T)$  by considering a sequence of normal stellar atmospheres spanning a range of effective temperatures. This is best done using theoretical models, since databases of observed stellar spectra are inhomogeneous with respect to metallicity and surface gravity, and have uncertainties in  $T_{\text{eff}}$  for each star. Note that in this paper we are not trying to estimate equivalent widths exactly. We are interested in relative changes as a function of effective temperature (and, in Section 4, of centre-to-limb position).

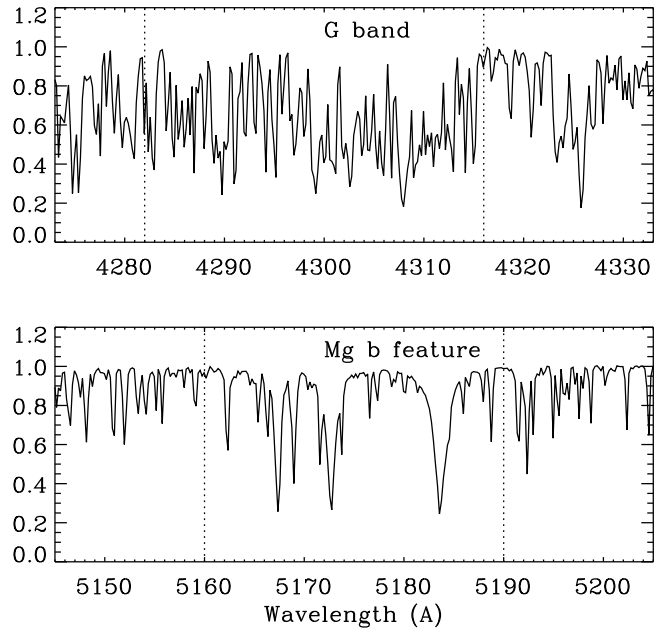


**Figure 1.** Synthetic spectra of the G band and the Mg b feature for a model atmosphere having  $T_{\text{eff}} = 5800$  K. Equivalent widths were estimated by measuring the total flux in the regions enclosed by dashed lines.

We have used the theoretical model GRS88 (Fuhrmann et al. 1993) to calculate spectra of  $H\alpha$ ,  $H\beta$ , Ca II K, the Ca II H + H $\epsilon$  blend and the 4383 Å Fe I line. Line profiles for the Balmer transitions were precalculated by K. Butler and T. Schöning (private communication) using VCS theory (Vidal et al. 1970). We have also calculated spectra of the G band and the Mg b feature (see Figure 1) using the LTE code RAI11 by M. Spite, as extended for molecular lines by Barby (1982) — see Barby (1981, 1982) and Cayrel et al. (1991) for descriptions of the atomic and molecular data bases. The model atmospheres used in this case are from Gustafsson et al. (unpublished).

For all models we have adopted solar surface gravity and metallicity; calculations of the  $H\alpha$  line by Fuhrmann et al. (1993) indicate that changing these parameters has little effect on equivalent widths. The microturbulent velocity was assumed to be 1 km/s (note this value is not critical for the strong lines we are considering) and the damping constants were obtained by fitting to the solar spectra (and also the Arcturus spectrum, for the G band and Mg b). The models do not include the chromospheric temperature inversion, but chromospheric effects should have negligible influence on the equivalent widths of the metal lines considered here because only the innermost line cores are formed at  $\log \tau_{5000} < -3.5$ . For the Balmer line, equivalent widths near the limb *are* significantly influenced by non-LTE effects in the line core, as discussed in Section 4.1 below.

The upper panel in Figure 2 shows  $W(T_{\text{eff}})$  as measured from our synthetic spectra. The lower panel shows the slope  $(\partial \ln W / \partial \ln T_{\text{eff}})$ , which we obtained simply by measuring the differences between adjacent points in the upper panel. The slope for the Balmer lines is 5–7, consistent with the value of 6 adopted by KBVF, which was based on published models (Kurucz 1979; Gray 1992). We see that the Mg b feature is especially promising for oscillation measurements.

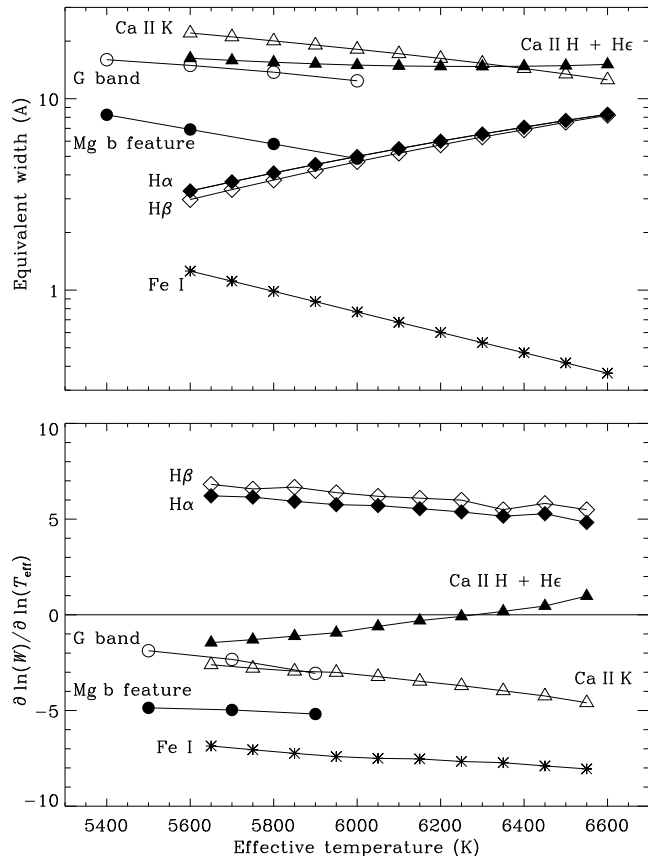


**Figure 2.** Equivalent width and slope  $(\partial \ln W / \partial \ln T_{\text{eff}})$  for various lines as a function of stellar effective temperature, based on model atmosphere calculations.

The Fe I lines are also useful since, although they are individually weaker, they are numerous and very sensitive to temperature.

### 3 OSCILLATIONS IN TARGET STARS

In the Sun, the amplitudes of individual oscillation modes can vary considerably over timescales of several days. However, different modes vary independently and the maximum amplitude, taken over all modes, stays roughly constant. When the solar oscillations are measured in bolometric luminosity, this amplitude is  $(\delta L/L)_{\text{bol}} = 4.1$  ppm (parts-per-million) — see Kjeldsen & Bedding (1995; hereafter referred to as KB) and references therein.

From KB, equations 5 and 7, amplitudes of solar-like oscillations in other stars should scale roughly as

$$(\delta L/L)_{\text{bol}} = \frac{L/L_{\odot}}{(M/M_{\odot})(T_{\text{eff}}/5777 \text{ K})} 4.1 \text{ ppm.} \quad (2)$$

This luminosity variation is due almost entirely to changes in temperature (the change in radius is negligible). Therefore, using  $L \propto R^2 T^4$  and Equation 1 we can write

$$\frac{\delta W}{W} = \frac{\partial \ln W}{\partial \ln T_{\text{eff}}} \frac{L/L_{\odot}}{(M/M_{\odot})(T_{\text{eff}}/5777 \text{ K})} 1.0 \text{ ppm.} \quad (3)$$

Equation 3 gives an estimate for the oscillation signal expected from equivalent-width measurements of a spectral

**Table 1.** Expected oscillations signal from observations of H $\alpha$  equivalent width for a sample of bright stars

| HR   | Name              | Spectral Type | $V$   | $T_{\text{eff}}$ (K) | $L$ ( $L_{\odot}$ ) | $M$ ( $M_{\odot}$ ) | $W$ ( $\text{\AA}$ ) | $\delta W/W$ (ppm) | $S/N$ | $\nu_{\text{max}}$ ( $\mu\text{Hz}$ ) | $\Delta\nu_0$ ( $\mu\text{Hz}$ ) | $\nu_{\text{rot}} \sin i$ ( $\mu\text{Hz}$ ) |
|------|-------------------|---------------|-------|----------------------|---------------------|---------------------|----------------------|--------------------|-------|---------------------------------------|----------------------------------|--|
| 2943 | $\alpha$ CMi      | F5IV-V        | 0.38  | 6500                 | 7.1                 | 1.60                | 7.7                  | 20                 | 10.7  | 1050                                  | 56                               | 0.7  |
| 5235 | $\eta$ Boo        | G0IV          | 2.68  | 6050                 | 9.5                 | 1.60                | 5.2                  | 32                 | 5.0   | 600                                   | 36                               | 1.1  |
| 8974 | $\gamma$ Cep      | K1III-IV      | 3.21  | 4850                 | 13.6                | 1.45                | 1.2                  | 83                 | 4.8   | 200                                   | 14                               | < 0.7  |
| 544  | $\alpha$ Tri      | F6IV          | 3.41  | 6350                 | 10.8                | 1.65                | 6.9                  | 31                 | 3.9   | 650                                   | 39                               | 7.8  |
| 5459 | $\alpha$ Cen A    | G2V           | -0.01 | 5770                 | 1.5                 | 1.09                | 4.0                  | 8                  | 3.7   | 2300                                  | 106                              | -  |
| 6380 | $\eta$ Sco        | F3III-IVp     | 3.33  | 6650                 | 9.6                 | 1.60                | 8.7                  | 25                 | 3.7   | 850                                   | 48                               | 14.7   |
| 3775 | $\theta$ UMa      | F6IV          | 3.17  | 6450                 | 9.4                 | 1.70                | 7.5                  | 25                 | 3.7   | 800                                   | 46                               | 1.1  |
| 8961 | $\lambda$ And     | G8III-IV      | 3.82  | 4900                 | 14.0                | 1.50                | 1.3                  | 81                 | 3.7   | 200                                   | 14                               | < 0.8  |
| 6212 | $\zeta$ Her       | G0IV+G7V      | 2.90  | 5800                 | 5.8                 | 1.30                | 4.2                  | 27                 | 3.3   | 700                                   | 42                               | < 1.0  |
| -    | Sun 1 pc          | G2V           | -0.15 | 5777                 | 1.0                 | 1.00                | 4.0                  | 6                  | 3.0   | 3050                                  | 135                              | 0.5  |
| 566  | $\chi$ Eri        | G8III         | 3.70  | 5250                 | 9.9                 | 1.65                | 2.2                  | 45                 | 2.8   | 350                                   | 24                               | -  |
| 7957 | $\eta$ Cep        | K0IV          | 3.43  | 5100                 | 7.9                 | 1.50                | 1.7                  | 42                 | 2.6   | 350                                   | 24                               | < 1.1  |
| 5986 | $\theta$ Dra      | F8IV          | 4.01  | 6250                 | 7.8                 | 1.50                | 6.3                  | 26                 | 2.4   | 750                                   | 45                               | 2.6  |
| 98   | $\beta$ Hyi       | G2IV          | 2.80  | 5800                 | 2.7                 | 0.99                | 4.1                  | 17                 | 2.1   | 1150                                  | 64                               | -  |
| 8665 | $\xi$ Peg         | F6III-IV      | 4.19  | 6300                 | 6.3                 | 1.40                | 6.7                  | 22                 | 1.9   | 900                                   | 52                               | 0.8  |
| 7602 | $\beta$ Aql       | G8IV          | 3.71  | 5250                 | 5.6                 | 1.40                | 2.1                  | 30                 | 1.8   | 550                                   | 33                               | < 1.3  |
| 7061 | 110 Her           | F6V           | 4.19  | 6450                 | 6.3                 | 1.55                | 7.5                  | 19                 | 1.7   | 1100                                  | 60                               | 1.6  |
| 963  | $\alpha$ For      | F8V+G7V       | 3.90  | 6250                 | 4.0                 | 1.30                | 6.3                  | 16                 | 1.5   | 1300                                  | 69                               | -  |
| 458  | $\nu$ And         | F8V           | 4.09  | 6200                 | 4.4                 | 1.30                | 5.9                  | 17                 | 1.5   | 1150                                  | 62                               | 1.0  |
| 3579 | -                 | F5V+G5V       | 4.11  | 6550                 | 3.8                 | 1.13                | 8.0                  | 15                 | 1.5   | 1400                                  | 77                               | 3.9  |
| 8430 | $\iota$ Peg       | F5V           | 3.76  | 6550                 | 3.7                 | 1.30                | 8.0                  | 13                 | 1.5   | 1650                                  | 84                               | 1.1  |
| 1136 | $\delta$ Eri      | K0IV          | 3.54  | 5100                 | 3.2                 | 1.10                | 1.7                  | 24                 | 1.4   | 650                                   | 40                               | < 1.7  |
| 1543 | $\pi^3$ Ori       | F6V           | 3.09  | 6650                 | 2.5                 | 1.30                | 8.5                  | 8                  | 1.3   | 2600                                  | 118                              | 3.3  |
| 5404 | $\theta$ Boo      | F7V           | 4.05  | 6300                 | 3.8                 | 1.30                | 6.7                  | 14                 | 1.3   | 1450                                  | 75                               | 4.8  |
| 4540 | $\beta$ Vir       | F9V           | 3.61  | 6150                 | 2.8                 | 1.20                | 5.7                  | 12                 | 1.3   | 1650                                  | 83                               | 0.5  |
| 6623 | $\mu$ Her         | G5IV          | 3.42  | 5550                 | 2.2                 | 1.00                | 3.0                  | 15                 | 1.3   | 1150                                  | 64                               | 2.8  |
| 5933 | $\gamma$ Ser      | F6V           | 3.85  | 6400                 | 3.3                 | 1.30                | 7.1                  | 12                 | 1.2   | 1700                                  | 85                               | 1.2  |
| 8969 | $\iota$ Psc       | F7V           | 4.13  | 6300                 | 3.2                 | 1.25                | 6.5                  | 13                 | 1.1   | 1600                                  | 81                               | 0.9  |
| 799  | $\theta$ Per      | F8V           | 4.12  | 6350                 | 2.7                 | 1.25                | 6.9                  | 10                 | 0.9   | 1950                                  | 95                               | 1.0  |
| 937  | $\iota$ Per       | G0V           | 4.05  | 6000                 | 2.4                 | 1.15                | 5.0                  | 12                 | 0.9   | 1700                                  | 85                               | < 1.6  |
| 1983 | $\gamma$ Lep      | F6V           | 3.60  | 6450                 | 1.8                 | 1.25                | 7.3                  | 7                  | 0.8   | 3100                                  | 135                              | 2.3  |
| 5460 | $\alpha$ Cen B    | K1V           | 1.33  | 5350                 | 0.5                 | 0.90                | 2.4                  | 4                  | 0.7   | 4450                                  | 179                              | -  |
| 6927 | $\chi$ Dra        | F7V           | 3.57  | 6350                 | 1.8                 | 1.50                | 6.9                  | 6                  | 0.7   | 3450                                  | 139                              | 2.2  |
| 7665 | $\delta$ Pav      | G6-8IV        | 3.56  | 5500                 | 1.1                 | 0.90                | 2.9                  | 9                  | 0.7   | 2050                                  | 100                              | -  |
| 7936 | $\psi$ Cap        | F4V           | 4.14  | 6600                 | 1.8                 | 1.25                | 8.2                  | 6                  | 0.6   | 3300                                  | 142                              | 8.1  |
| 219  | $\eta$ Cas        | G0V+dM0       | 3.45  | 6100                 | 1.1                 | 1.15                | 5.4                  | 5                  | 0.6   | 3750                                  | 154                              | < 1.4  |
| -    | Sun 10 pc         | G2V           | 4.85  | 5777                 | 1.0                 | 1.00                | 4.0                  | 6                  | 0.3   | 3050                                  | 135                              | 0.5  |
| 509  | $\tau$ Cet        | G8V           | 3.50  | 5600                 | 0.4                 | 0.90                | 3.3                  | 3                  | 0.3   | 5650                                  | 218                              | 0.7  |
| 1084 | $\varepsilon$ Eri | K2V           | 3.73  | 5180                 | 0.3                 | 0.85                | 2.0                  | 3                  | 0.2   | 5350                                  | 206                              | < 5.4  |

line. The photon noise, on the other hand, scales as the square root of the number of photons detected in the line. Hence, assuming photon noise to be the dominant noise source, the signal-to-noise ratio for a fixed observing time will scale as:

$$S/N \propto \frac{\partial \ln W}{\partial \ln T_{\text{eff}}} \frac{L\sqrt{W} 10^{-0.2m}}{MT_{\text{eff}}}, \quad (4)$$

where  $m$  is the stellar magnitude at the relevant wavelength.

We have applied Equations 3 and 4 to a sample of bright stars that are likely to undergo solar-like oscillations. Table 1 shows fundamental parameters and expected oscillation characteristics for the stars, which were selected from *The Bright Star Catalogue* (Hoffleit 1982) to have  $V < 4.2$  and  $0.35 < B - V < 1.2$ . A further restriction to include only main-sequence stars and subgiants was made on the basis of

density, as described below. We also omitted known variables (e.g.,  $\delta$  Scuti stars) and close binaries having nearly-equal components. For the remaining binaries we give the parameters for the primary only (except  $\alpha$  Cen, whose components are listed separately).

For the Sun,  $\alpha$  Cen A and B, Procyon ( $\alpha$  CMi),  $\eta$  Boo,  $\beta$  Hyi and  $\varepsilon$  Eri we adopted the same fundamental parameters as used in KB and KBVF. For the other stars, we estimated effective temperatures using  $T_{\text{eff}} \simeq 11000 \text{ K}/(B - V + 1.24)$ , used parallaxes from *The Bright Star Catalogue* and took bolometric corrections from Lang (1992). We made no reddening corrections except for HR 1543, which has  $E(B - V) = 0.03$ . Masses were estimated using stellar models in Fig. 1 of Bressan et al. (1993), which assumes solar metallicity, OPAL opacities and convective overshoot.

For each star we used Equation 3 to calculate the oscillation signal expected from observations of equivalent-width fluctuations of H $\alpha$ . Computing similar results for other lines is straightforward using the data in Figure 2. The predictions for  $\eta$  Boo and the Sun agree roughly with the Balmer-line observations of KBVF, although the amplitude scale in Table 1 may need revision once more observations become available (we are currently analysing high-quality data from  $\alpha$  Cen A, Procyon and the Sun). However, the relative amplitudes of the stars should not change drastically unless Equation 2, which is based on theoretical models, is found to be incorrect.

The stars in Table 1 are ordered according to  $S/N$ . This is the signal-to-noise ratio for a fixed observing time, arbitrarily normalized to give  $S/N = 3$  for the Sun at a distance of 1 pc. How much observing time would this require? Based on the KBVS observations of  $\eta$  Boo, a total of  $1.4 \times 10^{10}$  photons/Å are required to produce a photon-noise level of 10 ppm. This allows us to estimate the observing time required to achieve a given  $S/N$ . For example, a 2.5-metre telescope collecting photons with a total efficiency of 5% would take about 43 hours to achieve the  $S/N$  given for each star in Table 1. This estimate is based on observations at H $\alpha$  only – simultaneous measurement of other spectral lines would improve matters. Also, we have neglected  $1/f$  noise sources, such as instrumental drift, which will be important for stars oscillating at low frequencies (i.e., sub-giants).

The ranking of targets in Table 1 may differ for the other observing techniques (luminosity and velocity) and can be calculated using the formulae in KB. The Table also includes rough estimates for the frequency of maximum oscillation amplitude  $\nu_{\max}$  and the large frequency separation  $\Delta\nu_0$ , computed by scaling from the Sun (see KB). These frequencies will be important when choosing targets and designing observing programs. The large separation depends on the average density of the star and the table only includes stars for which  $\Delta\nu_0 > 1/(\text{day}) = 11.57 \mu\text{Hz}$ , in order to restrict the sample to main-sequence stars and subgiants.

The table also shows the quantity

$$\nu_{\text{rot}} \sin i = v \sin i / (2\pi R) \quad (5)$$

$$\simeq 0.23 \mu\text{Hz} \frac{v \sin i / \text{km s}^{-1}}{R/R_{\odot}}, \quad (6)$$

where  $\nu_{\text{rot}}$  is rotation frequency of the star. Components of an oscillation mode that is split by stellar rotation will be separated by approximately  $\nu_{\text{rot}}$  (see below).

Finally, it is worth mentioning the double-lined spectroscopic binary  $\alpha$  Equ (HR 8131), whose components (G5 III and A5 V) are slightly too faint to be included in Table 1. The masses and luminosities of both components have been derived from interferometric and spectroscopic observations by Armstrong et al. (1992), making this system particularly valuable for testing stellar models.

## 4 MODE SENSITIVITY

### 4.1 Calculations

From equivalent-width observations of the daytime sky, KBVF detected solar oscillations with degrees  $\ell = 0, 1, 2$  and 3. The detection of  $\ell = 3$  was puzzling, given that the

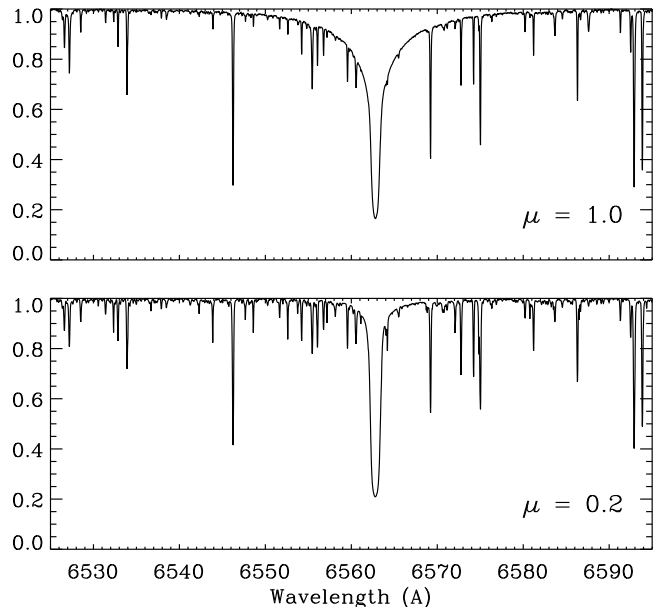


**Figure 3.** Observed H $\alpha$  spectra of the Sun at the centre and edge of the disk, taken from Brault & Testerman (1972). The wings of the H $\alpha$  line are much weaker in the lower diagram, whereas the metal lines and the core of H $\alpha$  show little variation.

the observations did not resolve the solar disk. The answer is straightforward: the Balmer lines are much weaker at the edge of the solar disk than at the centre (see Figure 3), so their integrated profiles are strongly weighted towards the disk centre. This has led us to investigate in detail the sensitivity of the equivalent-width method to modes with different values of  $\ell$ .

The calculation involves integrating the oscillations over the stellar surface, including the effects of limb darkening (Christensen-Dalsgaard & Gough 1982; Heynderickx et al. 1994; Robinson et al. 1995). The oscillations of a star can be described in terms of spherical harmonics  $Y_{\ell}^m(\theta, \phi)$ . If the star is rotating slowly, there is no preferred direction and we are free to choose a coordinate system with the polar axis pointed towards the observer. In this case, all integrations of spherical harmonics will be zero unless  $m = 0$ . Even for stars in which rotation is important, the following analysis is still useful, as discussed at the end of this section.

For  $m = 0$ , the spatial response function for each  $\ell$  (the ratio of the observed to the actual amplitude) is

$$S_{\ell} = 2\sqrt{2\ell + 1} \int_0^1 P_{\ell}(\mu) I(\mu) F(\mu) \mu d\mu. \quad (7)$$

Here  $\mu = \cos \theta$ ,  $P_{\ell}(\mu)$  is the Legendre polynomial of degree  $\ell$ ,  $I(\mu)$  is the centre-to-limb variation of continuum intensity (classical limb darkening) and  $F(\mu)$  is the centre-to-limb variation of the oscillation signal.

The function  $I(\mu)$  for the Sun is well approximated by

$$I(\mu) = 1 - u_2(1 - \mu) - v_2(1 - \mu^2), \quad (8)$$

where the coefficients vary with wavelength (Allen 1973). The function  $F(\mu)$  depends on how the observations are made. If the oscillations are observed via the Doppler shift of a spectral line then  $F(\mu) = \mu$ , corresponding to the projection of a nearly-radial pulsation along the line of sight.

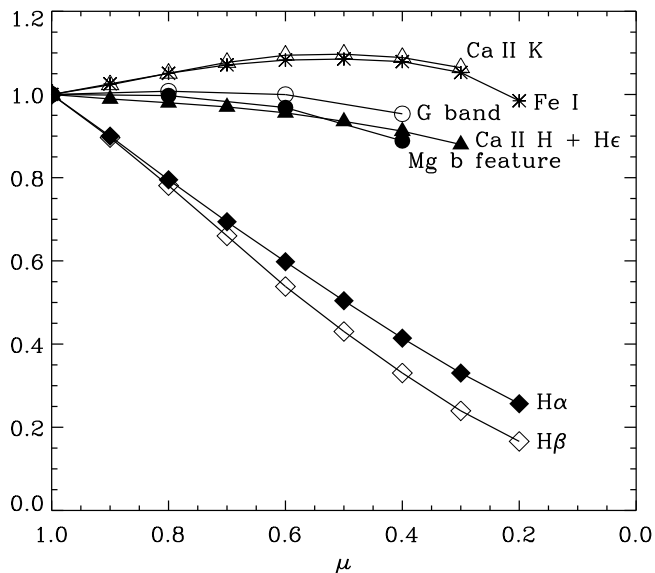


**Figure 4.** Centre-to-limb variation of equivalent width from solar-temperature model atmospheres, normalized to unity at the centre of the disk.

For observations in intensity there is no projection effect (to a good approximation) and  $F(\mu) = 1$ . If the oscillations are observed in equivalent width then we set  $F(\mu) = W(\mu)$ , the spatial variation of equivalent width from centre to limb.

In principle, we could determine the function  $W(\mu)$  from spatially-resolved spectra of the Sun. However, at visible wavelengths it seems that only two have been published: the *Preliminary Kitt Peak Photoelectric Atlas* (Brault & Testerman 1972), which has spectra at  $\mu = 1.0$  and  $\mu = 0.2$  (see Figure 3), and the atlas by Delbouille et al. (1973), which contains a single spectrum at  $\mu = 1.0$ .

To estimate  $W(\mu)$  at all values of  $\mu$ , we have therefore used the models described in Section 2 to produce intensity spectra at different points on a stellar disk. The results for a star with solar temperature, normalized to the disk centre, are shown in Figure 4. For the Balmer line cores, non-LTE effects are important and the models significantly underestimated the area of the line cores near the limb. To account for this, we assumed the difference between the actual equivalent width and that predicted by the GRS88 model increases linearly with decreasing  $\mu$ . Based on the measurements of  $W(\mu)$  at two points on the solar disk ( $\mu = 1.0$  and  $0.2$ ), we could correct the GRS88 equivalent widths at all intermediate points (the correction at  $\mu = 0.3$  was 35% for  $H\alpha$  and 18% for  $H\beta$ ). The final values are shown in Figure 4.

For those lines that were computed using the GRS88 model, we have repeated the calculations using the semi-empirical model of Holweger & Müller (1974). For the Balmer lines, we again corrected the equivalent widths for the missing core area. The resulting  $W(\mu)$  profiles for all lines are similar to those in Figure 4, to within 10%.

One other comparison with observation is possible. Quoting the unpublished *Michigan Atlas*, Holweger (1967) gives equivalent widths at  $\mu = 1.0$  and  $\mu = 0.3$  for many lines, including  $5172 \text{ \AA}$  Mg I and  $4383 \text{ \AA}$  Fe I (but note that his values for Ca II H & K and H I come from model calculations). For these lines, the ratio  $W(\mu = 0.3)/W(\mu = 1.0)$  given by Holweger agrees with our calculations to within

10%. It would clearly be desirable to have detailed centre-to-limb measurements of all these strong lines, similar to those of the  $7774 \text{ \AA}$  O I triplet by Altrock (1968) and King & Boesgaard (1995).

Our general conclusion is that the Balmer lines are strongly limb darkened, while the other lines have almost constant strength from centre to limb. For our purposes, it is sufficient to approximate  $F(\mu)$  for each spectral line using a linear function:

$$F(\mu) = 1 - c(1 - \mu). \quad (9)$$

By fitting a straight line to each set of points in Figure 4 (giving more weight to the central portion of the disk, since this contributes the greatest area), we obtained the following values for  $c$ : 0.95 for  $H\alpha$ , 1.0 for  $H\beta$  (which we also adopt for  $H\gamma$  and  $H\delta$ ),  $-0.2$  for Ca II K, 0.1 for the Ca II H + He blend,  $-0.2$  for Fe I, 0.05 for the G band and 0.15 for the Mg b feature.

Our Balmer-line models indicate that  $c$  varies quite slowly with effective temperature ( $c \propto T_{\text{eff}}^{-0.5}$ ), so the results given here apply to a broad class of stars.

Having obtained approximations for  $I(\mu)$  and  $F(\mu)$ , we can now integrate Equation 7. Results for the five lowest-degree modes ( $\ell = 0, \dots, 4$ ) are:

$$\begin{pmatrix} S_0 \\ S_1 \\ S_2 \\ S_3 \\ S_4 \end{pmatrix} = \begin{pmatrix} 1 & \frac{2}{3} & \frac{1}{2} & \frac{2}{5} \\ \frac{2}{\sqrt{3}} & \frac{\sqrt{3}}{2} & \frac{2\sqrt{3}}{5} & \frac{1}{\sqrt{3}} \\ \frac{\sqrt{5}}{4} & \frac{4}{3\sqrt{5}} & \frac{\sqrt{5}}{4} & \frac{8}{7\sqrt{5}} \\ 0 & \frac{\sqrt{7}}{12} & \frac{4}{5\sqrt{7}} & \frac{\sqrt{7}}{8} \\ -\frac{1}{8} & 0 & \frac{3}{32} & \frac{16}{105} \end{pmatrix} \times \begin{pmatrix} 1 - c & c - 1 & c - 1 \\ c & 1 - 2c & -c \\ 0 & c & 1 - c \\ 0 & 0 & c \end{pmatrix} \times \begin{pmatrix} 1 \\ u_2 \\ v_2 \end{pmatrix} \quad (10)$$

This matrix product, which should be evaluated from right to left, can be used to estimate the mode sensitivity of each observing method as a function of wavelength. Note that Equation 10 can be used for velocity measurements by setting  $c = 1$  and for intensity measurements by setting  $c = 0$ .

## 4.2 Results and discussion

Figure 5 shows the sensitivities as calculated from Equation 10, expressed relative to  $\ell = 0$ . In the case of velocity and intensity observations (solid and dotted curves), there are published solar oscillation data with which to compare the calculations:

(i) Observations in velocity from the South pole using the Na I line (590 nm) by Grec et al. (1980) give  $S_1/S_0 = 1.5$ ,  $S_2/S_0 = 1.2$ ,  $S_3/S_0 = 0.6$  and  $S_4/S_0 = 0.2$  (the scatter is about  $\pm 0.2$ ).

(ii) Observations in bolometric intensity from the Solar Maximum Mission by Woodard & Hudson (1983) give  $S_1/S_0 = 1.25$  and  $S_2/S_0 = 0.83$  (scatter about  $\pm 0.06$ ).

(iii) Observations in luminosity with the IPHIR green channel (500 nm) by Toutain & Fröhlich (1992) give  $S_1/S_0 = 1.09$  and  $S_2/S_0 = 0.79$  (scatter about  $\pm 0.07$ ).

In each case, there is good agreement with our results.

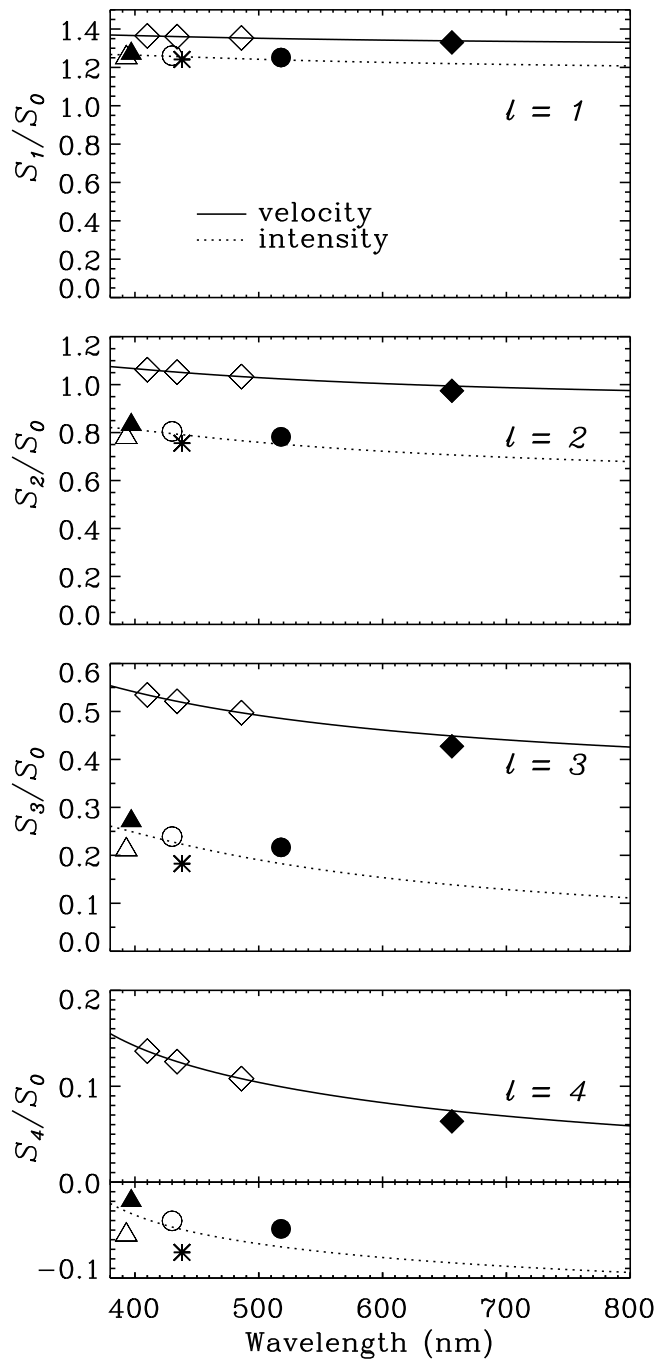


**Figure 5.** Sensitivity of observing methods as a function of wavelength. The solid line is for observations in velocity and the dashed line for intensity. Individual points indicate equivalent-width observations in different spectral features, with symbols having the same meaning as in Figures 2 and 4 (but with the addition of H $\gamma$  and H $\delta$ , shown as open diamonds). Negative values of  $S_\ell$  mean the oscillations will appear to have reversed phases.

Turning to equivalent-width measurements, we see from Figure 5 that the Balmer lines give a response similar to that of velocity measurements. This follows from their strong centre-to-limb variation and is consistent with the solar observations by KBVF — in particular, we can now explain their detection of  $\ell = 3$ . The other absorption lines considered here have much weaker centre-to-limb variations ( $c \simeq 0$ ;

see Figure 4) and so have spatial responses similar to that of intensity measurements. This suggests the possibility of determining the  $\ell$  value of a given mode using simultaneous observations in several absorption lines, which might be interesting for studies of  $\delta$  Scuti variables (Matthews 1993).

Finally, we consider a rotating star. A mode with a particular  $(n, \ell)$  will split into a multiplet having  $m = -\ell, \dots, \ell - 1, \ell$ , with the components being separated by about  $\nu_{\text{rot}}$  (the oscillation power summed over these peaks is conserved). If the star is seen pole-on, only modes with  $m = 0$  are observable and the analysis of this section holds exactly: we would not notice that the star is rotating. At the other extreme, in a star seen from near the equator (e.g., the Sun) the modes with  $|\ell - m|$  odd will have zero amplitude because the Legendre function is antisymmetric around the equator. For  $\ell = 1$  we would therefore only see two modes ( $m = \pm 1$ ). The total power will be the same as for a non-rotating star, so the amplitudes of these two modes will each be multiplied by  $1/\sqrt{2}$  relative to the non-rotating case. For  $\ell = 2$  we would see three modes ( $m = -2, 0$  and  $2$ ) with relative amplitudes of  $\sqrt{3/2}$ ,  $1/2$  and  $\sqrt{3/2}$ . Other cases can readily be calculated using the formulae given by Christensen-Dalsgaard (1994).

## ACKNOWLEDGMENTS

We are grateful to the following for useful discussions: Richard Altrock, Lawrence Cram, Bob Fosbury, Jeremy King, Barry LaBonte, Bill Livingston, Ruth Peterson and Dick White. We thank the referee for some important suggestions and Robert Kurucz for supplying the *Preliminary Kitt Peak Photoelectric Atlas* in electronic form.

## References

- Allen, C.W., 1973, *Astrophysical Quantities*, London: Athlone Press, third edition
- Altrock, R.C., 1968, *Sol. Phys.* 5, 260
- Armstrong, J.T., Mozurkewich, D., Vivekanand, M., Simon, R.S., Denison, C.S., & Johnston, K.J., 1992, *AJ* 104, 241
- Barbuy, B., 1981, *A&A* 101, 365
- Barbuy, B., 1982, PhD thesis, Univ. Paris VII
- Bedding, T.R., & Kjeldsen, H., 1995, More on solar-like oscillations in  $\eta$  Boo. In: Stobie, R.S., & Whitelock, P.A. (eds.), *IAU Colloquium 155: Astrophysical Applications of Stellar Pulsation*, Vol. 83 of *A.S.P. Conf. Ser.*, p. 109, Brigham Young, Utah
- Brault, J.W., & Testerman, L., 1972, *Preliminary Kitt Peak Photoelectric Atlas*, Tucson: Kitt Peak Natl. Obs.
- Breger, M., 1975, *ApJ* 201, 653
- Bressan, A., Fagotto, F., Bertelli, G., & Chiosi, C., 1993, *A&AS* 100, 647
- Brown, T.M., & Gilliland, R.L., 1994, *ARA&A* 33, 37
- Cayrel, R., Perrin, M.N., Barbuy, B., & Buser, R., 1991, *A&A* 247, 108
- Christensen-Dalsgaard, J., 1994, *Lecture Notes on Stellar Oscillations*, Institut for Fysik og Astronomi, Aarhus Universitet, third edition
- Christensen-Dalsgaard, J., & Gough, D.O., 1982, *MNRAS* 198, 141

- Christensen-Dalsgaard, J., Bedding, T.R., Houdek, G., Kjeldsen, H., Rosenthal, C., Trampedach, R., Monteiro, M., & Nordlund, Å., 1995a, Near-surface effects in modelling oscillations of  $\eta$  Boo. In: Stobie, R.S., & Whitelock, P.A. (eds.), *IAU Colloquium 155: Astrophysical Applications of Stellar Pulsation*, Vol. 83 of *A.S.P. Conf. Ser.*, p. 447, Brigham Young, Utah
- Christensen-Dalsgaard, J., Bedding, T.R., & Kjeldsen, H., 1995b, *ApJ* 443, L29
- Delbouille, L., Roland, G., & Neven, L., 1973, *Spectrophotometric Atlas of the Solar Spectrum from  $\lambda 3000$  to  $\lambda 10000$* , Liège: Inst. d'Astrophysique
- Frandsen, S., 1984, Intensity oscillations in spectral lines in the Sun. Theory and observation. In: *Theoretical Problems in Stellar Stability and Oscillations*, p. 303, Université de Liège
- Fuhrmann, K., Axer, M., & Gehren, T., 1993, *A&A* 271, 451
- Gray, D.F., 1992, *The observation and analysis of stellar photospheres*, Vol. 20 of *Cambridge Astrophysics Series*, Cambridge: Cambridge University Press, 2nd edition
- Gre, G., Fossat, E., & Pomerantz, M.A., 1980, *Nat* 288, 541
- Heynderickx, D., Waelkens, C., & Smeyers, P., 1994, *A&AS* 105, 447
- Hoffleit, D., 1982, *The Bright Star Catalogue*, Yale University Observatory, New Haven
- Holweger, H., 1967, *Z. Astrophys.* 65, 365
- Holweger, H., & Müller, E.M., 1974, *Sol. Phys.* 39, 19
- King, J.R., & Boesgaard, A.M., 1995, *AJ* 109, 383
- Kjeldsen, H., & Bedding, T.R., 1995, *A&A* 293, 87, (KB)
- Kjeldsen, H., Bedding, T.R., Viskum, M., & Frandsen, S., 1995, *AJ* 109, 1313, (KBVF)
- Kurucz, R.L., 1979, *ApJS* 40, 1
- Lang, K.R., 1992, *Astrophysical Data: Planets and Stars*, Springer-Verlag
- Matthews, J.M., 1993, Observing the eigenmodes of  $\delta$  Scuti and roAp stars. In: Brown, T.M. (ed.), *GONG 1992: Seismic Investigation of the Sun and Stars*, Vol. 42 of *A.S.P. Conf. Ser.*, p. 303, Brigham Young, Utah
- Robinson, E.L., Mailloux, T.M., Zhang, E., Koester, D., Stiening, R.F., Bless, R.C., Percival, J.W., Taylor, M.J., & van Citters, G.W., 1995, *ApJ* 438, 908
- Toutain, T., & Fröhlich, C., 1992, *A&A* 257, 287
- Vidal, C.R., Cooper, J., & Smith, E.W., 1970, *J. Quant. Spectrosc. Radiat. Transfer* 10, 1011
- Woodard, M., & Hudson, H., 1983, *Nat* 305, 589

This paper has been produced using the Blackwell Scientific Publications L<sup>A</sup>T<sub>E</sub>X style file.